DOI: 10.1177/0003702818809474

Atmospheric Aerosol Multiband Synthesis Imaging Spectrometer

Xiaoxu Wang[1,2], Zihui Zhang[1],*, Shurong Wang[1], Yu Huang[1], Guanyu Lin[1], Zhanfeng Li[1], Xiaohu Yang[1]

[1]*State Key Laboratory of Applied Optics, Changchun Institute of Optics, Fine Mechanics and Physics, Chinese Academy of Sciences, Changchun, 130033, China.*

[2]*University of Chinese Academy of Sciences, Beijing, 100049, China.*

*zhangzihui123@126.com

Abstract

According to the characteristics of the spectrum distribution for atmospheric aerosol detection, a multiband synthesis imaging spectrometer system based on Czerny–Turner configuration is designed and proposed in this paper. Using a grating array instead of a traditional single grating, and together with a filter array, the proposed configuration can achieve hyperspectral imaging with the spectral resolution of 0.16 nm, 0.24 nm, 0.29 nm, and 2.05 nm respectively in the spectral bands of 370 nm–430 nm, 640 nm–680 nm, 840 nm–880 nm, and 1560 nm–1660 nm. Firstly, the system aberration caused by the spectral change was eliminated based on Rowland circle theory, and then Zemax software was used to optimize and analyze the optical design. The analysis results show that the root mean square (RMS) of the spot diagram is less than 9 μm in all the working spectral bands, which demonstrates that the aberration has been corrected and a good imaging quality can be achieved. This design of multiband synthesis imaging spectrometer configuration proves to be not only feasible, but also simple and compact, which lays a solid foundation for the practical application in the field of atmospheric aerosol remote sensing spectroscopy.

Keywords: Aerosol detection, optical design of instruments, spectrometers, spectroscopic instrumentation

Introduction

Atmospheric aerosol refers to the solid and liquid particles suspended in the atmosphere whose diameters are in the range of 0.01 μm~100 μm, which is one of the most active components of the atmosphere.[1] Atmospheric aerosol primarily affects the climate, environment, and the accuracy of quantitative remote sensing, and has gradually become a serious problem which

DOI: 10.1177/0003702818809474

affects the survival of human beings and social development. Conducting the detection of the global distribution of atmospheric aerosol is of great significance for studying aerosol retrieval and prediction. However, due to the great changes of the types and quantities of atmospheric aerosol in time and space, it is always difficult to achieve global atmospheric aerosol detection or retrieval.[2]

Due to the complexity of the atmospheric composition, the working spectral bands of atmospheric aerosol detectors need to cover several important spectral wavebands in the spectral range of 360 nm–1700 nm.[3,4] Now there mainly exist two kinds of aerosol detectors: the multiband imager and the broadband imaging spectrometer. The multiband imager uses filters to select the wavelengths of light. It has a low spectral resolution and less spectral channels, resulting in low accuracy for aerosol retrieval. The imaging spectrometer has a wider working spectral range, but requires the use of multichannel configuration, making its optical configuration large and complex.[5]

In view of the disadvantages of the traditional aerosol detection instruments, a novel multiband synthesis imaging spectrometer which adopts the grating tiling technology and can achieve aerosol detection from ultraviolet (UV) to near infrared (NIR) with only one imaging spectrometer is designed and proposed in this paper. The design proves to be feasible and effective through analysis and evaluation described in the following sections.

Spectral Bands for Aerosol Detection

The aerosol retrieval process is shown in Fig. 1.

<Insert Fig. 1 here>

Assuming that the observation target is a Lambert body with a bidirectional reflectance of R_s, considering the multiple reflections between the upper and the underlying surfaces of the atmosphere, the apparent reflectance R observed by satellites can be expressed as:[6]

$$R(\theta_0,\theta,\varphi) = R_a(\theta_0,\theta,\varphi) + \frac{F(\theta_0)T(\theta)R_s(\theta_0,\theta,\varphi)}{1-SR_s(\theta_0,\theta,\varphi)} \quad (1)$$

DOI: 10.1177/0003702818809474

where θ_0 is the solar zenith angle; θ is the viewing zenith angle of the instrument; φ is the relative azimuth angle of the sun and the instrument; R_a is the atmospheric path radiance, namely, the bidirectional reflectance of the atmosphere; F is the atmospheric downward transmittance; T is the atmospheric upward transmittance in the viewing direction of the remote sensing instrument; S is the atmospheric backscattering rate (in practical application, $S = R_a$).

The radiance of the atmosphere can be acquired with the atmospheric backscattering rate. According to Eq. 1, there are three problems that need to be solved for aerosol retrieval based on remote sensing data: first, the recognition and removal of the cloudy area; second, the removal of the reflection signal from the earth surface; third, the effects of the atmospheric scattering and absorption. In order to observe clouds, marine, terrestrial, and absorptive aerosols, and earth surface reflectance, the working spectral bands of atmospheric aerosol detecting instruments should cover five spectral ranges: 380 nm, 410 nm, 670 nm, 865 nm, and 1610 nm.[7] By comparing and calculating the signals and the minimum reflectance of different spectral bands, the extent of cloud cover and the aerosol optical thickness in the atmosphere can be retrieved.[8]

Aberration Analysis and Correction for Czerny–Turner Optical Configuration

In the history of spectroscopic instruments, the Czerny–Turner system is the most widely used optical configuration due to its simple and compact structure, which is as shown in Fig. 2. The incident light from the entrance slit is first collimated by the collimating mirror, then dispersed by the plane grating and finally imaged on the focal plane by the focus mirror. The image in the direction parallel to the slit is corresponding to the images of the slit, which is the spatial dimension; and the image in the direction perpendicular to the slit is corresponding to different spectral images of the slit, which is the spectral dimension.[9]

<Insert Fig. 2>

As the C–T system is a reflective optical system, it suffers no axial chromatic aberration, and lateral aberration is only due to the desired grating, only spherical aberration, coma, and astigmatism need to be considered and optimized respectively.

Spherical Aberration

The spherical aberration affects not only the spatial resolution, but also the spectral resolution of the imaging spectrometer, so it should be controlled within the tolerance of the aberration.

DOI: 10.1177/0003702818809474

According to the Rayleigh criterion,[11] the wavefront aberration W_s generated by the spherical aberration should be smaller than λ/4, that is:

$$W_{s(max)} = \frac{(y_{max})^4}{8r^3} \leq \frac{\lambda}{4} \quad (2)$$

where y_{max} is the semi-aperture of the collimating mirror, λ is the wavelength and r is the curvature radius of the collimating mirror. It can be seen from Eq. 2 that limiting the numerical aperture of the incident light beam can effectively reduce the spherical aberration.

Coma

For the C–T configuration, both the collimating mirrors and the focusing mirrors are placed off-axis, which will introduce coma. As shown in Fig. 2, according to Beulter's and Allemand's theories,[12,13] the coma generated by the collimating mirror and the focusing mirror when the incident light is off-axis can be calculated respectively. The total coma of C–T system is the sum of the two, which can be expressed as:

$$\Delta = \Delta_1 + \Delta_2 = \frac{3W^2 r_2 \cos^2\theta \cos(\alpha_2/2)}{8\cos^3(\alpha_1/2)} \cdot \left[\frac{\sin(\alpha_2/2)\cos^2\theta\cos^3(\alpha_1/2)}{r_2^2\cos^2 i\cos^3(\alpha_2/2)} - \frac{\sin(\alpha_1/2)\cos i}{r_1^2\cos\theta}\right] \quad (4)$$

where W is the diameter of the collimated beam, r_1 and r_2 are respectively the curvature radii of the collimating mirror and the focusing mirror, α_1 and α_2 are respectively the off-axis angles of the collimating mirrors and the focusing mirrors, i and θ are respectively the incident angle and the diffraction angle of the grating. If coma Δ = 0, from Eq, 3 a new equation can be derived

$$\frac{\sin(\alpha_2/2)}{\sin(\alpha_1/2)} = \frac{r_2^2\cos^3 i}{r_1^2\cos^3\theta}\left[\frac{\cos(\alpha_2/2)}{\cos(\alpha_1/2)}\right]^3 \approx \frac{r_2^2}{r_1^2}\left(\frac{\cos i}{\cos\theta}\right)^3 \quad (4)$$

According to Eq. 4, we can learn that coma can be corrected by choosing the focusing mirror with an appropriate off-axis angle.

Astigmatism

DOI: 10.1177/0003702818809474

As shown in Fig. 3, astigmatism is mainly caused by the different focal lengths of the mirrors in the meridian and sagittal directions.

<Insert Fig. 3 here>

When a spherical mirror is illuminated by parallel light with an incident angle of α/2, the focal lengths in the meridian direction and sagittal directions, respectively[14,15]

$$f_t' = (r/2)\cos(\alpha/2) \quad (5)$$

$$f_s' = (r/2)/\cos(\alpha/2) \quad (6)$$

Therefore, in a C–T optical system the difference between the focal lengths respectively in the meridian direction and sagittal directions can be expressed as:

$$\Delta f' = (f_{s1}' - f_{t1}') + (f_{s2}' - f_{t2}') \quad (7)$$

As seen in Eq. 7, eliminating the astigmatism means $\Delta f'=0$. So toroidal focus can be used to correct the astigmatism.

Broad Spectral Band Aberration

When the grating is illuminated by the collimated light, the incident angle i is a constant. According to grating Eq. 8:

$$d(\sin i + \sin\theta) = m\lambda \quad (8)$$

where m is the diffraction order of the grating. The incident light will be dispersed into monochromatic light beams of different wavelengths with different reflection angles. As shown in Fig.4, the light beams of different wavelengths are respectively incident on the points A, O, and B of the focusing mirrors, whose incident angles are respectively $\alpha_2'/2$, $\alpha_2/2$ and $\alpha_2''/2$.

<Insert Fig. 4 here>

According to Eqs. 5, 6, and 7, there exist differences among the off-axis angles of the light of different wavelengths reflected by the focusing mirror, which is the key factor that affects the correction of the broad spectral band aberrations. According to Roland's circular

DOI: 10.1177/0003702818809474

theory, if the grating is located on the Roland circle of the focusing mirrors, the incident angles of the light beams emitted from point G to the focusing mirror are approximately equal. At this time, according to the geometric relationship, line C_2G is perpendicular to line GO, so the distance between the center of the grating and the focusing mirror is: $L_{gf} = r_2\cos(\alpha_2/2)$. Thus, by adjusting the optical configuration parameters to the same, the broad spectral band aberration is corrected, which means the effects of different wavelengths on the aberration are eliminated.[17]

The principle of the Grating Array

According to the aberration analysis above, when the grating is illuminated by collimated light and placed on the Roland circle of the focusing mirror, the effects of different wavelengths on the imaging spectrometer aberration can be eliminated. Based on this, a grating array that replaces the grating in traditional C–T configuration is designed to eliminate the aberration, as shown in Fig. 5.

<Insert Fig. 5 here>

The grating array is a combination of several rectangular gratings with different groove densities and blaze angles. According to the requirement of aerosol detection discussed in section 2, the working band of the imaging spectrometer needs to cover the spectral ranges of 380 nm, 410 nm, 670 nm, 865 nm, and 1610 nm. One grating is enough for 380 nm and 410 nm, due to the relatively small difference between them, and another three gratings are needed respectively for 670 nm, 865 nm and 1610 nm. The four gratings are combined to form a grating array. According to Eq. 8, by controlling the groove densities of the gratings strictly, a small shift of the diffraction angles of the gratings can be generated, thus the light beams reflected by different gratings can be imaged by focusing mirror on different positions of the flat-panel detector. To avoid the mutual interference among the different spectral signals of the light diffracted by different gratings, several bandpass filters with different central wavelengths and bandwidths are needed to cover the corresponding gratings respectively. According to the detecting spectral bands and the grating distribution of the grating array, the parameters of the bandpass are designed as shown in Table I.

Design of the Multiband Synthesis Imaging Spectrometer

DOI: 10.1177/0003702818809474

According to the aberration correction method and the spectral band distribution characteristics for aerosol detection, a new multiband synthesis imaging spectrometer was designed (see Table I for the working spectral bands) with an entrance slit of 3.4 mm×12 μm and a numerical aperture (NA) of 0.083 (f=6). As the working spectral range of the designed spectrometer covers from UV to NIR, two kinds of detectors are needed.

Ray tracing and system optimization were implemented using Zemax; the optical path of the designed imaging spectrometer is shown in Fig. 6. The multiband synthesis imaging spectrometer consisted of an entrance slit, a spherical collimating mirror, a grating array, two plane mirrors, a toroidal focusing mirror, and two detectors, where one of the plane mirrors was used to change the direction of the NIR light. The boundary dimension of the designed imaging spectrometer was calculated to be 185 mm×150 mm×35 mm through software analysis, which is pretty compact.

<Insert Fig. 6 here>

Figure 7 shows the spot diagram on the image plane of the imaging spectrometer system. As seen in Fig. 7, the root mean square (RMS) of the dispersed spots for different wavelengths and viewing angles are all less than 9 μm, which demonstrates that the aberration of the system has been well corrected; and as shown in Fig. 8, the modulation transfer function (MTF) of the system for the central wavelengths of each sub-gratings all reach the diffraction limit. Therefore, it can be concluded that the image quality is good.

<Insert Fig. 7 here>

<Insert Fig. 8 here>

Figure S1 (online Supplemental Material) shows the spectrum distribution on the surface of the two detectors. There are three spectra on the surface of detector1, which are generated respectively from grating1, grating2, and grating3 shown in Fig. 5, and the line resolution of the spectrum is 12.5 nm/mm, 18.2 nm/mm, and 22.1 nm/mm respectively. The lateral magnification of the imaging spectrometer system is 1.1, when the pixel size of the detector is 13 μm, the spectral resolutions of the three spectra imaged on detector1 are 0.16 nm, 0.24 nm, and 0.29 nm respectively. Similarly, when the pixel size of detector2 is 50 μm, the spectral resolution of the spectrum imaged on detector2 is 2.05 nm.

DOI: 10.1177/0003702818809474

<AUTHOR>The journal places a limit of no more than eight (8) figures in a paper (with the exception of review papers. Please move Fig. 9 (now Fig. S1) to Supplemental Material and cite accordingly in text.</AUTHOR>

Conclusion

To meet the requirements of detecting several discrete spectral bands in a wide spectral range for aerosol detection, a multiband synthesis imaging spectrometer based on the Czerny–Turner configuration was designed. By using the filter array and the grating array, the designed imaging spectrometer can achieve hyperspectral imaging detection in the spectral bands of 370 –430 nm, 640 –680 nm, 840–880 nm, and 1560–1660 nm. According to the aberration analysis of the imaging spectrometer using C–T configuration, the Roland circle theory was used to eliminate the aberration caused by the wide spectral range. Ray tracing and system optimization was implemented using Zemax, and the optimization result was analyzed. The results show that in the working spectral bands, the RMSs of the spot diagrams in the full field of view are all less than 9 μm and the MTFs can all reach the diffraction limits, which demonstrates that the aberration of the system has been well corrected.

In general, the proposed system has the following four characteristics: (i) By adjusting the diffraction angles of the gratings and the transmittance of the filters, the radiation power of each working spectral bands can be controlled effectively ensuring that the detectors can achieve their best signal-to-noise ratio working intervals. (ii) Choosing the appropriate gratings can improve the diffraction efficiency of each working spectral bands. (iii) The proposed optical configuration is simple and compact, whose boundary dimensions can be 185 mm×150 mm×35 mm, meanwhile it can achieve the hyperspectral imaging detection from ultraviolet to NIR. (iv) The proposed system has a high spectral resolution, which can achieve 0.16 nm, 0.24 nm, 0.29 nm and 2.05 nm respectively in the four working spectral bands.

The proposed design of the multiband synthesis imaging spectrometer was proven feasible through the analysis above, and will provide a technical guidance for the next air-based and space-based aerosol detection applications.

Funding

National Natural Science Foundation of China (NSFC) (11573025).

DOI: 10.1177/0003702818809474

Supplemental Material

All supplemental material mentioned in the text is available in the online version of the journal.

References

1. Z. Enyun, Ma Jiao. “The Present Situation of Aerosol Research in China”. Environmental Science and Management. 2008. 33(12): 57–59.
2. N. Jianhua, Z. Liming, C. Hongyao. “Influence of Atmospheric Model and Aerosol Type on Radiation Transfer Calculation”. Qiangjiguang Yu Lizishu [High Power Laser and Particle Beams]. 2010. 22(5): 983–986.
3. H. Xinli, G. Hangfa, Y. Tao, Z. Zhouwei, et al. “Effects of Aerosol Optical Thickness on the Optical Remote Sensing Imaging Quality”. Guangpuxue Yu Guangpu Fenxi [Spectrosc. Spectral Anal.]. 2014. 34(3): 28–32.
4. R.B. Husar, J.M. Prospero, L.L. Stowe. “Characterization of Tropospheric Aerosols over the Oceans with the NOAA Advanced Very High Resolution Radiometer Optical Thickness Operational Product”. J. Geophys. Res. 1997. 102: 16889–16909.
5. M.D. King, Y.J. Kaufman, D. Tanré, T. Nakajima. “Remote Sensing of Tropospheric Aerosols from Space: Past, Present and Future”. Bull. Am. Meteorol. Soc. 1999: 2229–2260.
6. M.S. Wong, J.E. Nichol. “Retrieval of Aerosol Optical Thickness Using MODIS 500×500 m^2, a Study in Hong Kong and Pearl River Delta Region”. IEEE Trans. Geosci. Remote Sens. 2010. 48(8): 3318–3327.
7. O.P. Torres, P.K. Bhartia, J.R. Herman, Z. Ahmad, et al. “Derivation of Aerosol Properties from Satellite Measurements of Backscattered Ultraviolet Radiation: Theoretical Basis”. Geophys. Res. 1998. 103(D14): 17099–17110.
8. N. Kikuchi, H. Ishida, M. Yoshida, H. Takenaka. “GOSAT TANSO-CAI L1B and L1B+ Products”. International Archives of the Photogrammetry, Remote Sensing, and Spatial Information Sciences. Kyoto, Japan; 9–12 August 2010. 38(8): 398–401. http://www.isprs.org/proceedings/XXXVIII/part8/pdf/W03P01_20100310224740.pdf [accessed 2 Oct 2018].
9. Q. Xue, S. Wang, F. Lu. "Aberration-Corrected Czerny–Turner Imaging Spectrometer with a Wide Spectral Region,” Appl. Optics. 2009. 48(1): 11–16.

DOI: 10.1177/0003702818809474

10. Q. Xue. The Study on Limb Imaging Spectrometer for Space-Based Atmospheric Remote Sensing. [Doctor of Engineering Dissertation]. Changchun, China: Changchun Institute of Optics, Fine Mechanics and Physics, Chinese Academy of Sciences, 2010.
11. Y. Daoyin, T. Hengying. Engineering Optics [Gong Cheng Guang Xue]. Beijing: China Machine Press. 1999. 4th ed. Pp. 169–170.
12. H.G. Beutler. "The Theory of the Concave Grating". J. Opt. Soc. Am. 1945. 35(5): 331–350.
13. C.D. Allemand. "Coma Correction in Czerny–Turner Spectrographs". J. Opt. Soc. Am. 1968. 58(2): 159–163.
14. Q.P. Remund, D. Newell, J.V. Rodriguez, S. Asbury, et al. "The Ozone Mapping and Profiler Suite (OMPS): On-Orbit Calibration Design". Proceedings Volume 5652, Passive Optical Remote Sensing of the Atmosphere and Clouds IV. 2004. 5652: 165–173. DOI: 10.1117/12.579016.
15. S.A. Goldstein, J.P. Walters. "A Review of Considerations for High-Fidelity Imaging of Laboratory Spectroscopic Sources—Part 1". Spectrochim. Acta, Part B. 1976. 31(4): 201–220.
16. Q. Xue, S. Wang, F. Lu. "Aberration-Corrected Czerny–Turner Imaging Spectrometer with a Wide Spectral Region". Appl. Optics. 2009. 48(1): 11–16.
17. L. Youping, Y. Bingxi, H. Changyuan, L. Zhu. "Tradeoff Optimization Design of Optical Configuration on Imaging Spectrometer". Guangxue Jingmi Gongcheng [Optics and Precision Engineering]. 2006. 14(6): 974–979.

DOI: 10.1177/0003702818809474

Captions

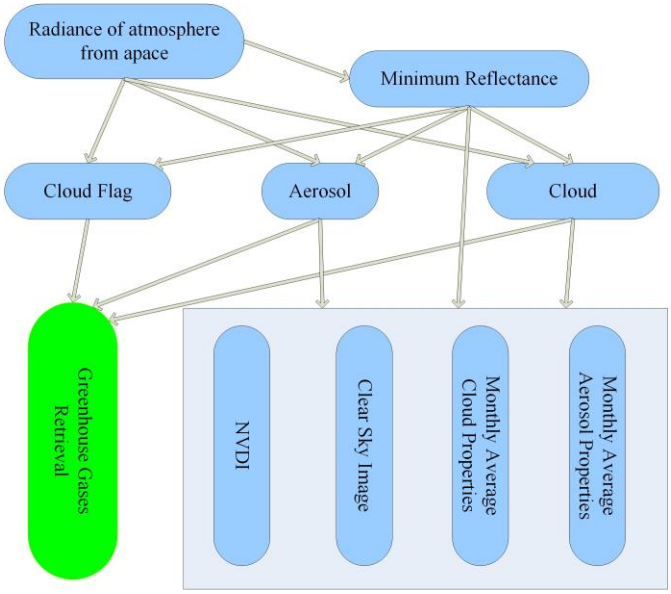

Fig. 1. The flowchart for aerosol retrieval.

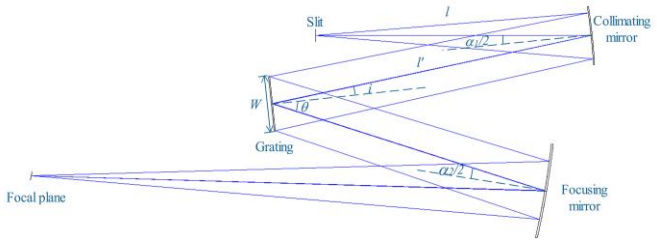

Fig. 2. The optical configuration of Czerny–Turner system. Reproduced with permission from Xue.[10]

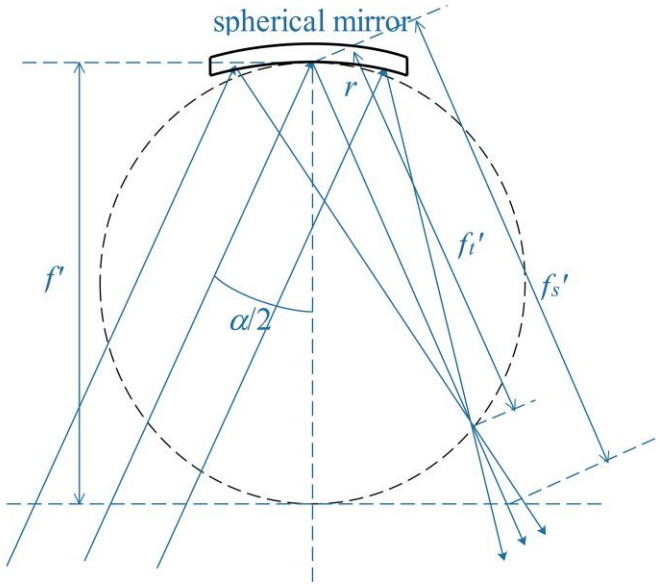

DOI: 10.1177/0003702818809474

Fig. 3. The astigmatism of spherical mirrors when illuminated by collimated beam. Reproduced with permission from Xue.[10]

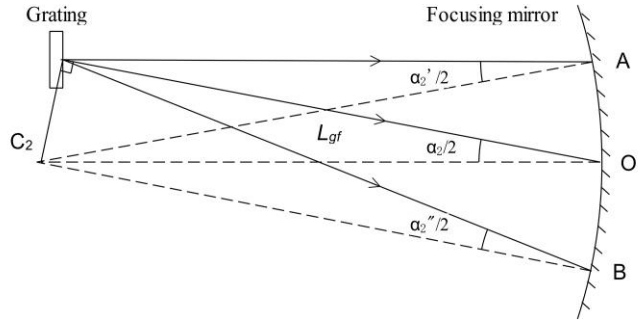

Fig. 4. The schematic diagram of the light path of grating dispersion. Reproduced with permission from Xue.[16]

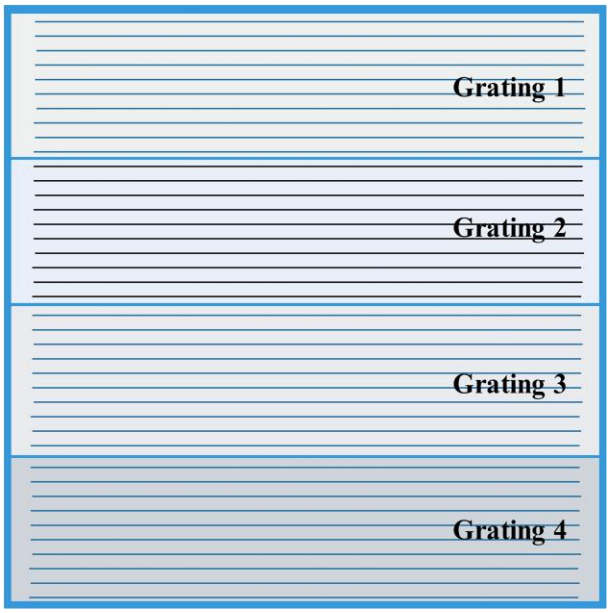

Fig. 5. The schematic diagram of the grating array.

DOI: 10.1177/0003702818809474

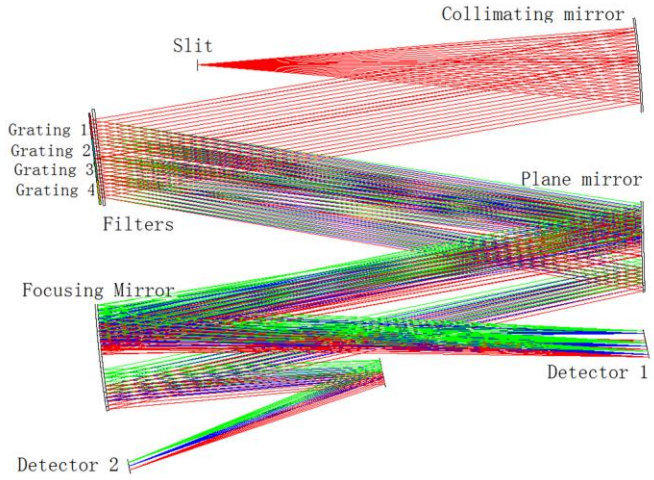

Fig. 6. The multiband synthesis imaging spectrometer (Fig. 5 shows the surface of the grating array, and the grating array shown in Fig. 6 is placed vertically to the direction of the grating array in Fig. 5).

DOI: 10.1177/0003702818809474

DOI: 10.1177/0003702818809474

Fig. 7. Spot diagram analysis result of the system by Zemax. The black circles present the diameter of a diffraction-limited image.

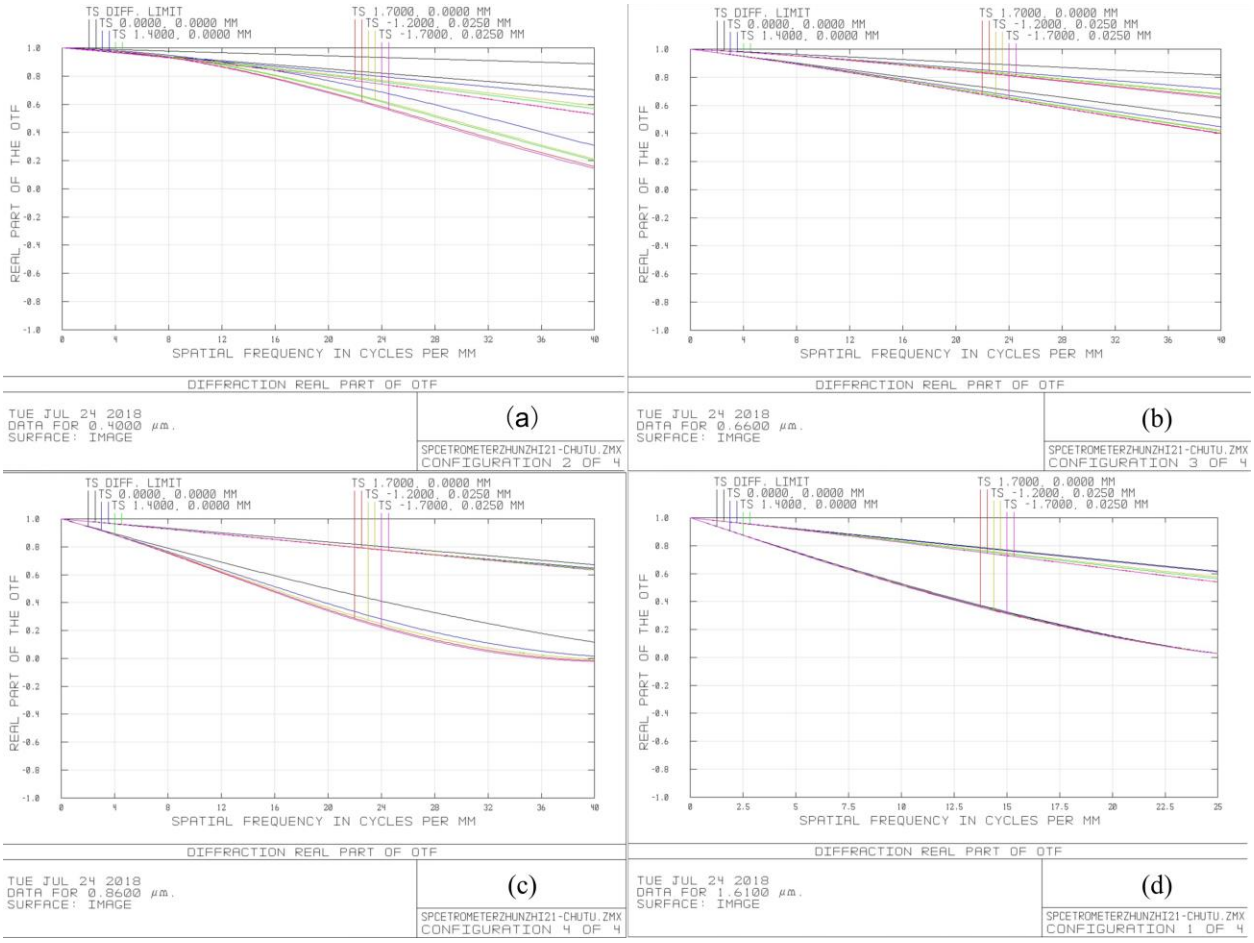

Fig. 8. MTF of the system for the central wavelengths of each sub-gratings: (a) 400 nm, (b) 660 nm, (c) 860 nm, (d) 1610 nm.

DOI: 10.1177/0003702818809474

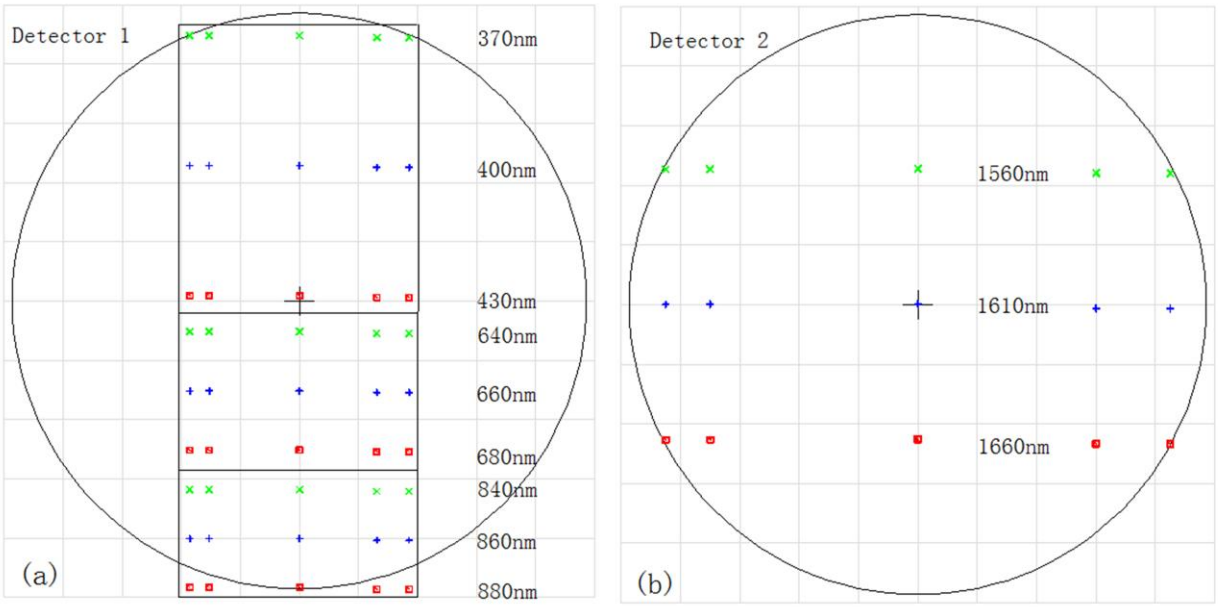

Fig. S1. The spectrum distribution on the two image planes.<**Please see note above regarding limits on figures. Please move to Supplemental Material and ensure the citation is correctly noted in text.**>

Table I. The spectral ranges of the filters.

Grating index	Spectral range (nm)
1	370–430
2	640–680
3	840–880
4	1560–1660